J Electr Eng Technol.2018; 13(1): 124-132
http://doi.org/10.5370/JEET.2018.13.1.124

ISSN(Print) 1975-0102
ISSN(Online) 2093-7423

A High Efficiency LLC Resonant Converter-based Li-ion Battery Charger with Adaptive Turn Ratio Variable Scheme

Yeong-Jun Choi*, Hyeong-Gu Han*, See-Young Choi*, Sang-Il Kim* and Rae-Young Kim†

Abstract – This paper proposes an LLC resonant converter based battery charger which utilizes an adaptive turn ratio scheme to achieve a wide output voltage range and high efficiency. The high frequency transformer of the LLC converter of the proposed strategy has an adaptively changed turn ratio through the auxiliary control circuit. As a result, an optimized converter design with high magnetizing inductance is possible, while minimizing conduction and turn-off losses and providing a regulated voltage gain to properly charge the lithium ion battery. For a step-by-step explanation, operational principle and optimal design considerations of the proposed converter are illustrated in detail. Finally, the effectiveness of the proposed strategy is verified through various experimental results and efficiency analysis based on prototype 300W Li-ion battery charger and battery pack.

Keywords: LLC resonant converter, Battery charger, High efficiency, Adaptive turn ratio, Wide output voltage

1. Introduction

Recently, various green transportations such as xEVs, E-bike, and E-scooter using batteries as a main power source, have expeditiously developed and penetrated the commercial marketplace. Generally, lithium-ion batteries are primarily used in such applications due to diverse reasons such as high energy densities, no memory effects and low self-discharge rates [1].

Meanwhile, the importance of the Li-ion battery charging system has also been increased to ensure safe and powerful use of the battery. Most charging systems employ a constant current-constant voltage (CC-CV) charging profile as displayed in Fig. 1 to prevent overcurrent and overcharge of the battery where the dashed line stands for a battery voltage V_{batt} and the solid line stands for the battery charging current I_{batt} [2]. As can be seen from the figure, the terminal voltage of the battery is widely varied from the cut-off voltage to the maximum charging voltage during the entire charging process; hence, Li-ion battery chargers should cover a wide output voltage range.

LLC resonant converter is a promising high-efficiency battery charger candidate possessing several advantages [3-5]. The converter inherently achieves zero voltage switching (ZVS) of the primary side switches and soft commutation capability of semiconductor devices over the whole operational range. Therefore, the turn-on loss is small and the reverse recovery loss of the diode is reduced, so that a high switching frequency operation is possible and the power density of the entire system can be increased. Additionally the magnetic elements of the resonant tank can be integrated into a single transformer core, which is advantageous in terms of cost.

However, the LLC resonant converter also possesses a handicap as a battery charger: There is a trade-off in the design methodology to achieving high efficiency and meeting wide output voltage variations to cover wide variations in battery terminal voltage. To achieve a wide output voltage range, the LLC resonant converter need to operate at a frequency lower than the resonant frequency. However, such operation decreases efficiency due to the presence of a large circulating current. Moreover, a small magnetizing inductance of the resonant tank is usually required; therefore, efficiency became worse due to an excessive turn-off loss and magnetizing current. Hence, the optimal design of an LLC resonant is realized to be a delicate process [6].

To overcome this problem, several studies have been performed [7-15]. One solution is to develop a design method for resonant tanks to meet a given battery voltage and efficiency specification. [7-12]. However, these studies only reveal the inherent trade-off relationship limitation that cannot naturally be overcome. In the literature, a strategy of using auxiliary windings was proposed to realize a wide output voltage [13]. However, since this method was proposed for hold-up compensation, so there is no focus on maintaining the ZVS condition, and it is difficult to apply it to a battery charger. Some other researches discussed solutions for high power applications such as 3.3kW or 6.6kW [14, 15]. The main concept of these studies is to integrate the many advantages of two or more DC-DC converters with topology modification. However, it is impossible to apply results of these researches directly for low power applications below 500W.

† Corresponding Author: Dept. of Electrical and Biomedical Engineering, Hanyang University, Korea. (rykim@hanyang.ac.kr)
* Dept. of Electrical Engineering, Hanyang University, Korea. ({choi0jun, pehan09, si401}@hanyang.ac.kr, see781@naver.com,)
Received: February 16, 2017; Accepted: June 16, 2017

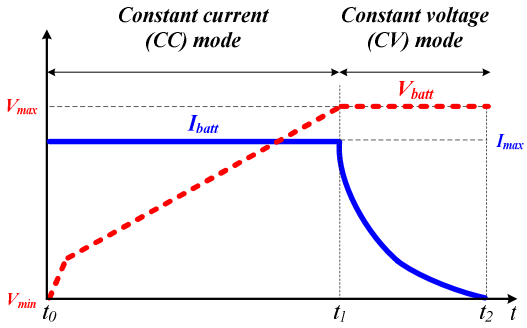

Fig. 1. CC-CV charging profile

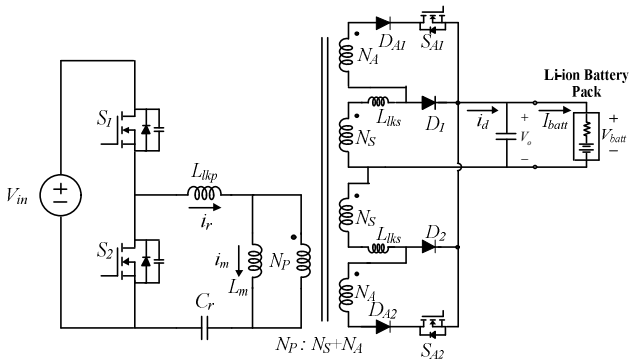

Fig. 2. Proposed LLC resonant converter

This paper proposes a high efficiency 300W Li-ion battery charger based on LLC resonant converter that uses an adaptive winding ratio scheme to guarantee a wide output voltage range. The proposed converter adopts a half-bridge converter for the step-down capability on the primary side and a center tap rectifier for the low forward voltage drop on the secondary side. The adaptive winding ratio method, which is controlled via the auxiliary circuit, enables high efficiency to be achieved under widely varied output voltages. By adopting adaptive winding ratio method, the magnetization inductance of the resonance tank can be designed to a large value. Therefore, the conduction and the switching off losses at the primary side are decreased, which means the total efficiency is improved.

The rest of this paper is organized as follows. In Section II, the proposed converter and operating mode analysis are described. In Section III, a design example is presented for a "given condition". In Section IV, experimental results which include waveforms and efficiency and analysis based on the results are presented to verify the effectiveness of the proposed method.

2. Proposed Battery Charger with an Adaptive Turn Ratio

2.1 Circuit description

The proposed battery charger can is displayed in Fig. 2. The first stage of the proposed charger is the same as an conventional half-bridge LLC resonant converter where V_{in} denotes the input voltage, S_1, S_2 denote the main switches, L_{lkp} and L_{lks} denote the leakage inductance of the primary side and the secondary side of the integrated transformer, i_r denotes the resonant current, L_m denotes the magnetizing inductance, i_m denotes the magnetizing current and C_r is the resonant capacitor. N_p denotes the number of the primary winding of the transformer. The secondary structure of the proposed charger is similar to conventional center tap rectifier. On the basis of the conventional structure, the transformer winding structure of secondary side is modified by adding additional windings and its auxiliary driving circuit, where N_S, N_A denote the number of turns with regard to the secondary and auxiliary windings, S_{A1}, S_{A2} denote the auxiliary switches, and D_1, D_2, D_{A1}, D_{A2} denote the rectifier and auxiliary diodes. These modified structures allowed the turn ratio of the transformer to be varied adjustably. For example, if S_{A1} and S_{A2} are turned on, the effective number of secondary winding is increased to the sum of N_S and N_A, that is defined as "high gain mode" in this paper. When S_{A1}, S_{A2} are turned off, the proposed charger operated with N_S turns, which is defined as "normal mode". The i_d, V_o, V_{batt} and i_{batt} stand rectified current, output voltage, battery voltage and the battery charging current respectably. In this paper, V_o and V_{batt} are assumed to be the same.

2.2 Operational principle

Fig. 3 displays the output voltage or voltage gain curve of the LLC resonant converter with respect to the switching frequency. As can be seen from the graph, when the operating frequency is changed, the output voltage is adjusted accordingly. Supposing that the Li-ion battery possesses a terminal voltage range between 25V and 42V as seen in Fig. 3, the LLC resonant converter satisfies this voltage range to realize the CC-CV charging profile.

$$M = \frac{2n \cdot V_o}{V_{in}} \tag{1}$$

$$M = \left| \frac{\left(\frac{\omega^2}{\omega_p{}^2}\right)\frac{k}{k+1}}{j\left(\frac{\omega}{\omega_o}\right)\cdot\left(1-\frac{\omega^2}{\omega_o{}^2}\right)\cdot Q\frac{(k+1)^2}{2k+1}+\left(1-\frac{\omega^2}{\omega_p{}^2}\right)} \right| \tag{2}$$

where, $k = \frac{L_m}{L_{lkp}}$, $Q = \frac{\sqrt{L_r / C_r}}{R_o}$, $\omega_o = \frac{1}{\sqrt{L_r C_r}}$,

$\omega_p = \frac{1}{\sqrt{L_p C_r}}$, $n = \frac{N_p}{N_S}$, $R_o = \frac{8n^2}{\pi^2}\frac{V_o}{I_{batt}}$, $L_p = L_M + L_{lkp}$,

$L_r = L_{lkp} + L_M \,||\, (n^2 L_{lks})$

Consequently, the converter has to be designed to cover

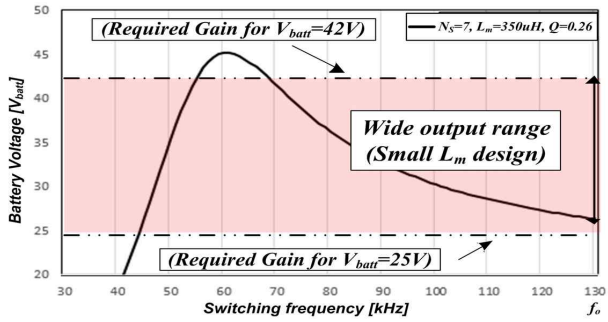

Fig. 3. Voltage gain curve of the conventional LLC resonant converter

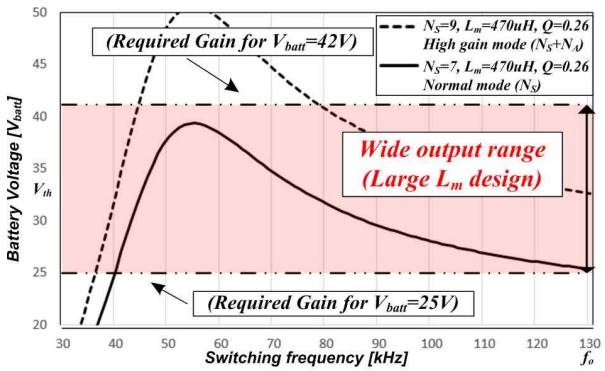

Fig. 4. Voltage gain curve of the proposed LLC resonant converter

the wide output voltage range capabilities.

Referring to (1), the voltage gain, M should be increased in order to obtain a wide range output voltage. Eq. (1) is expressed in detail in (2) where k is the ratio between L_m and L_{lkp}, Q denotes the quality factor, ω_o and ω_p denote the resonant angular frequencies, n denotes the turn ratio, R_o denotes the equivalent load resistance, L_p and L_r are the equivalent inductance that the secondary winding is open circuited or short-circuited respectively. [5, 16]. As can be seen from (2), Designing a small L_m is a simple solution to have a wide output voltage range. The smaller L_m becomes the smaller k as well, and resultantly, M increases However, this solution leads a deterioration of the overall efficiency of the converter due to the increased conduction and switch turn-off losses.

Fig. 4 displays the output voltage or voltage gain curve of the proposed LLC resonant converter. The converter with the proposed adaptive winding ratio technique has two different voltage gain curves: one is normal mode operation (indicated by a solid line) and the other is high gain operation (indicated by a dashed line). Under normal mode, the converter is not designed to achieve wide output voltage range. As a result, a large L_m that minimizes conduction losses and switch turn-off losses is used. On the other hand, when a high output voltage is necessary, high gain mode is operational. In this mode, the auxiliary switches S_{A1} and S_{A2} are turned on and the turn ratio of the transformer n increased from N_p/N_S to $N_p/(N_S+ N_A)$.

$$V_o = \frac{1}{2} \cdot \frac{1}{n} \cdot V_{in} \cdot M \tag{3}$$

Eq. (1) can be rearranged to generate (3). From (1) and (3), it is easily seen that a smaller n generates a higher voltage gain peak at the below resonant frequency, as displayed in Fig. 4; the required high output voltage is generated. On the other hand, a smaller M indicates that the switching frequency variation with regard to output voltage regulation during charging is decreased. Hence, the proposed scheme enables the battery charger to generate a higher voltage gain with a larger magnetizing inductance under a narrow switching frequency variation. Therefore, the RMS value of the resonant current, turn-off loss and circulating current period at the primary side are reduced.

2.3 Operating modes of the proposed LLC resonant converter

Fig. 5 displays the circuit diagram of two modes of operation of the proposed converter. When the threshold output voltage at which the operation mode is changed is expressed as V_{th} and the minimum and maximum output voltages are denoted as V_{min} and V_{max}, respectively the following analysis can be yield:

1) Normal mode [$V_{min} < V_{batt} < V_{th}$] : seen from Fig. 5(a), S_{A1}, S_{A2} are turned off and D_1, D_2 are forward biased.

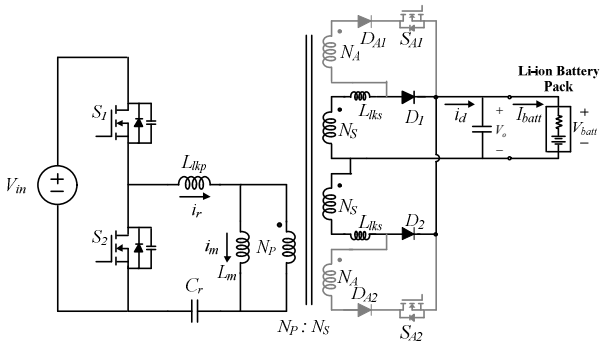

(a) Normal mode ($V_{min} \sim V_{th}$)

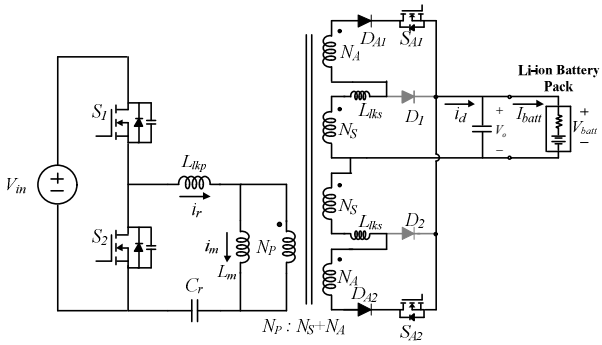

(b) High gain mode ($V_{th} \sim V_{max}$)

Fig. 5. Configuration of the proposed converter according to operational mode

The current flows through D_1 and D_2 like the conventional center-tap rectifier. The effective number of turns in the secondary side windings becomes N_S; as a result, the normal voltage gain is generated.

2) High gain mode [$V_{th} < V_{batt} < V_{max}$] : seen from Fig. 5(b), S_{A1}, S_{A2} are turned on simultaneously and the secondary side current does not continue to flow through the D_1 and D_2. The effective number of turns in the secondary side windings becomes ($N_S + N_A$). As a result, n is decreased to n_a; the turn ratio including auxiliary windings shown in (4). Consequently, a high output voltage is obtained by applying a reduced turn ratio. The increased output voltage can be confirmed by substituting n_a for n in (3).

$$n_a = \frac{N_p}{N_S + N_A} \tag{4}$$

2.4 Overshoot-less mode transition technique

If the auxiliary circuit on the secondary side is switched on during charging, an overshoot occurs in the primary side resonance current and the secondary side charging current. These transients cause stress and damage to the switch network or battery pack and require resolution. Therefore, this paper adopts an overshoot elimination algorithm depicted in Fig. 6(a). This algorithm temporarily increases the switching frequency first and then turns on the switch for the mode change to prevent overshooting as can be seen in Fig. 6(b).

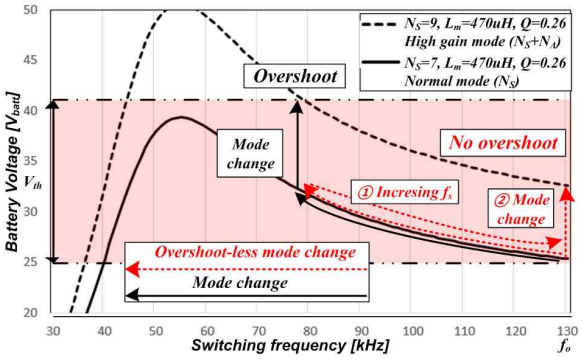

(a)

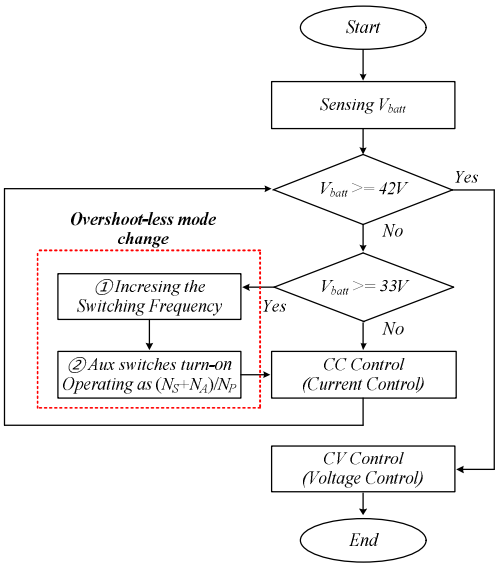

(b)

Fig. 6. The overshoot elimination algorithm: (a) the switching frequency trajectory; (b) A flow chart

Table 1. Design parameters

Item (Designator)	Conventional LLC converter [5]	Proposed LLC converter
Resonant Frequency (f_o)	130 kHz	130 kHz
Transformer Turn Ratio (N_P:N_S:N_A)	46 : 7	46 : 7 : 2
Magnetizing Inductance (L_m)	350 uH	470 uH
Resonant Inductor (L_r)	33 uH	33 uH
Resonant Capacitor (C_r)	23 nF	23 nF
Control Sampling Period	1 usec	1 usec
Mode Change Voltage (V_{th})	-	33V

3. Design Example

In order to explain the above sections briefly, a design example is presented based on Table 1. The electrical specifications of the converter in the design example are as follows: the nominal input voltage, V_{in} as 311V, the cut-off voltage of the battery, V_{batt_min} is 25V, the maximum charging voltage is 42V, and k is 10 with margin consideration. The charging current is determined to be 7A; the output power is 300W and the turn ratio of the normal mode is 6.5 where the converter operates at a resonant frequency f_o with a cut-off voltage of 25V.

3.1 Selection of turn ratio of transformer

The turn ratio of the transformer, n, needs to be suitably selected to maximize efficiency and provide DC gain appropriate from the maximum charging voltage to the cut-off voltage of the battery at the resonant frequency f_o. Considering the forward voltage drop of the secondary side diodes to be V_F, n is given to (5) where the DC gain at f_o is given as $M_{\omega_0} = (k+1)/k$ [5, 16]. Assuming V_F = 0.5V and substituting the given electrical specifications into (5) yields n = 6.5. The maximum voltage gain, M_{max}, is required to be 1.8 times larger than M_{wo} in order to regulate output voltage according to the given specifications. The quality factor Q is selected to be 0.25 in order to generate a high DC gain under normal mode.

$$n = \frac{N_p}{N_s} = \frac{V_{in}}{2(V_{bat\_min} + V_F)} \cdot M_{\omega_0} \tag{5}$$

3.2 Magnetizing inductance and the threshold voltage selection

The magnetizing inductance L_m is selected in consideration of the ZVS condition. To satisfy the ZVS condition, peak magnetizing inductor current, $i_{m,peak}$ of (6) should be able to discharge the parasitic output capacitance. This relationship can be expressed as (7) where C_{oss} is the parasitic output capacitance of the MOSFET, T_s is switching period, t_{dead} is dead time of the MOSFET. The large L_m is preferred in order to achieve the minimum conduction losses within the range satisfying (7) [17].

$$i_{m,peak} = \frac{nV_o}{L_m}\frac{T_s}{4} \tag{6}$$

$$L_m \le \frac{T_s \cdot t_{dead}}{16 \cdot C_{oss}} \tag{7}$$

However, an increase in L_m leads to an increase in k in (1), which leads to a decrease in the peak voltage gain. Hence, as shown in Fig. 7, under the range satisfying (4), the L_m is designed to be possible to generating the Mode Change Voltage V_{th} within the operating frequency of the converter (78 kHz~130 kHz). V_{th} is designed to be a median value of 33 V in consideration of the maximum charging voltage of the battery pack and the cut-off voltage.

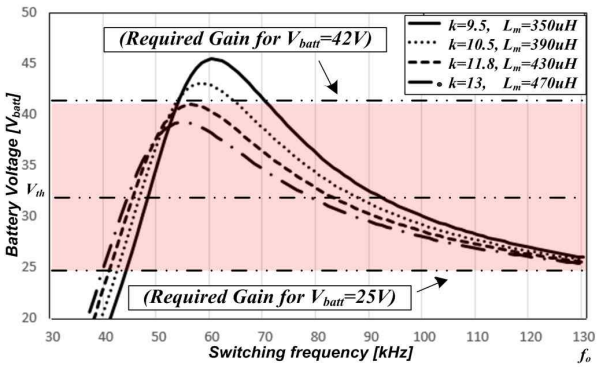

Fig. 7. Optimal magnetizing inductance (L_m) selection.

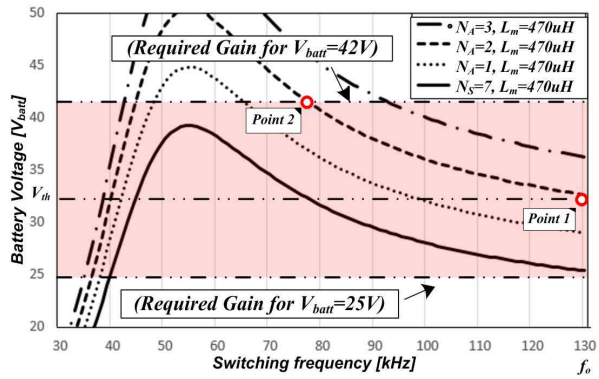

Fig. 8. Optimal number of turns of auxiliary winding selection

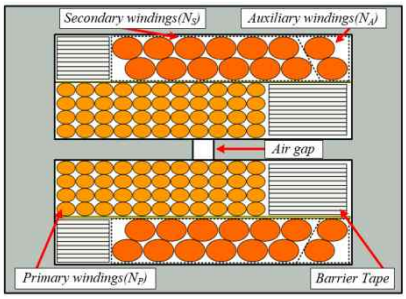

(a)

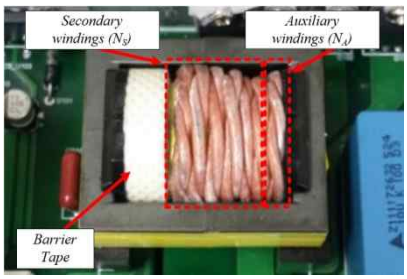

(b)

Fig. 9. An integrated transformer of the resonant tank: (a) winding structures and (b) a manufactured prototype

3.3 Determining the number of auxiliary windings

The number of the auxiliary winding turns, N_A, is optimized through the voltage gain curve as displayed in Fig. 8. By increasing N_A, M is increased due to the effect of the decreased n_a that is confirmed by substituting n_a for n in Eq. (2). The increased N_A and decreased n_a also affect the current flowing in the primary side; $i_{m,peak}$, RMS values of magnetizing current $i_{m,rms}$ and resonant current $i_{r,rms}$ as can be seen in (8), (9) and (10) [17]. As can be seen from these relationships, each value is proportional to the turn ratio of the transformer. Therefore, by applying the reduced n_a, $i_{m,peak@na}$, $i_{m,rms@na}$, $i_{r,rms@na}$ which are applied value of n_a, becomes smaller than $i_{m,peak@n}$, $i_{m,rms@n}$, $i_{r,rms@n}$ which are applied value of n and it leads an efficiency improvement.

In this paper, the N_A is selected to generate the same output voltage as V_{th} around the resonant frequency f_o (point 1), under consideration of satisfying a maximum charging

$$i_{m,peak@n} = \frac{nV_o}{L_m}\frac{T_s}{4} > i_{m,peak@n_a} = \frac{n_aV_o}{L_m}\frac{T_s}{4} \tag{8}$$

$$i_{m,rms@n} = \frac{1}{\sqrt{3}}\left(\frac{nV_o}{L_m}\frac{T_s}{4}\right) > i_{m,rms@n_a} = \frac{1}{\sqrt{3}}\left(\frac{n_aV_o}{L_m}\frac{T_s}{4}\right) \tag{9}$$

$$i_{r,rms@n} = \frac{1}{8}\frac{V_o}{nR_o}\sqrt{\frac{2n^4R_o^2T_s^2}{L_m^2}+8\pi^2} > i_{r,rms@n_a} = \frac{1}{8}\frac{V_o}{n_aR_o}\sqrt{\frac{2n_a^4R_o^2T_s^2}{L_m^2}+8\pi^2} \tag{10}$$

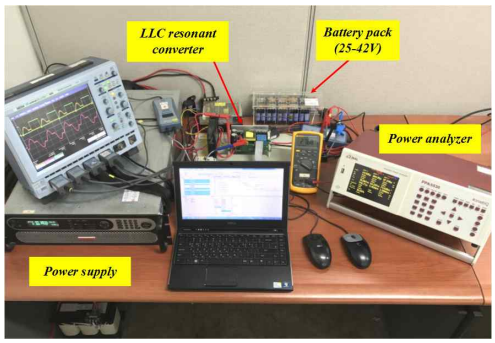

Fig. 10. Experimental setup of the prototype

voltage of 42V (point 2). In this example, with regard to selecting the optimal high gain mode case, choosing this mode satisfies the maximum voltage gain as well as the smallest increase in the number of secondary windings. As a result, N_A is selected to be 2 turns as seen in Fig. 7.

Figs. 9 (a) and (b) display the structure and design results of the integrated transformer using the EER 3542 magnetic core. As displayed in the Fig. 8(a), the number of the primary windings, N_P, secondary windings, N_S, and auxiliary windings, N_A are selected as 46, 7, and 2, respectively.

4. Performance Verification

In order to verify the effectiveness of the proposed converter, experiments based on the experimental set seen in Fig. 10 are performed based on the detailed parameters listed in Table 1. In the experiment, Cortex M-3 is used for digital control, and for the LLC resonant converter implementation, FSFR2100 and STPS20M100S are used. Figs. 11(a) and (b) display the steady-state waveforms of the conventional LLC resonant converter battery charger under 10% and 80% load conditions, respectively where V_{ds1} represents the drain source voltage of the S_1 and i_{ds1} represents the current flowing to S_1.

Figs. 12 (a) and (b) display the same waveforms for the proposed LLC resonant converter battery charger. As can be seen from the waveforms, the peak value of magnetization current is decreased from 1.28A to 0.77A under heavy condition; the turn-off current is decreased from 2A to 1.8A under light load conditions and from 1.1A to 0.8A under heavy load conditions. The measured resonant current RMS value is decreased from 1.55A to 1.48A under a light load and is decreased from 1.95A to 1.91A under a heavy load. Additionally, the circulating current period is also decreased from 7.77μs to 7.09μs and decreased from 6.84μs to 4.91 μs under light and heavy load condition respectively.

The reason for this numerical reduction can be attributed to a large L_m due to application of the proposed LLC resonant converter. Reduction of these factors reduces conduction and switching losses, leading to an improved

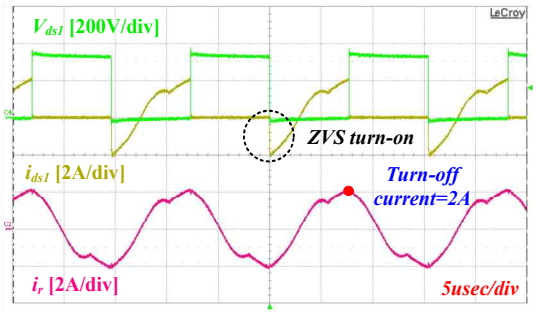

(a)

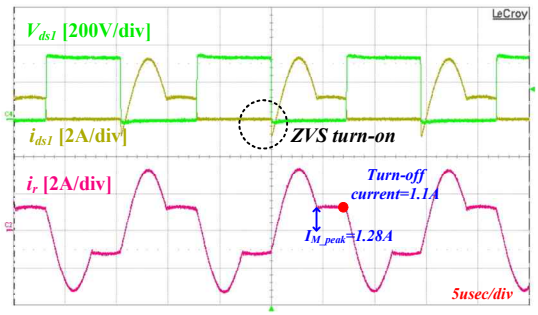

(b)

Fig. 11. Experimental result of the conventional LLC resonant converter: (a) at 10% load and (b) 80% load

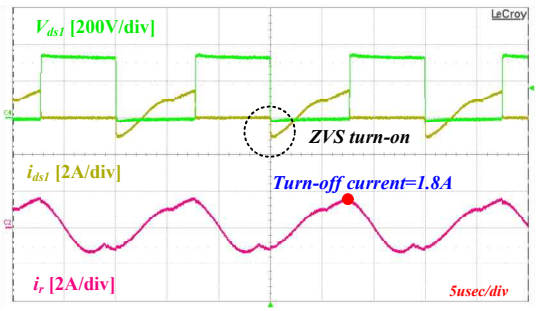

(a)

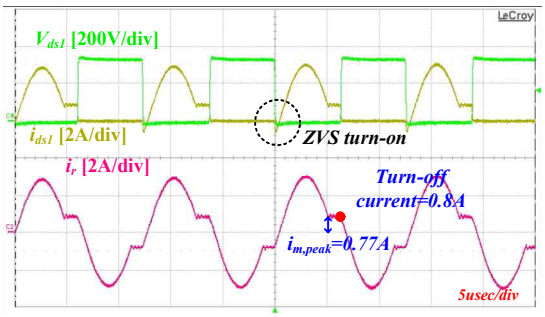

(b)

Fig. 12. Experimental result of the proposed LLC resonant converter: (a) at 10% load and (b) 80% load

efficiency shown in Fig. 13.

From the efficiency comparison result between the conventional LLC resonant converter and the proposed

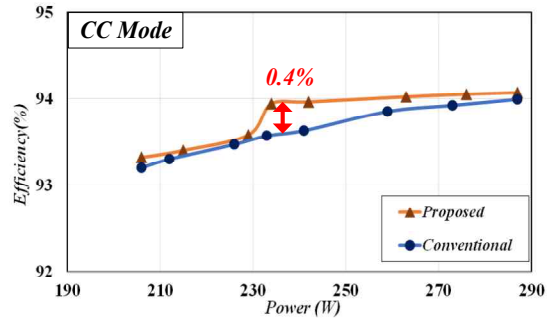

(a)

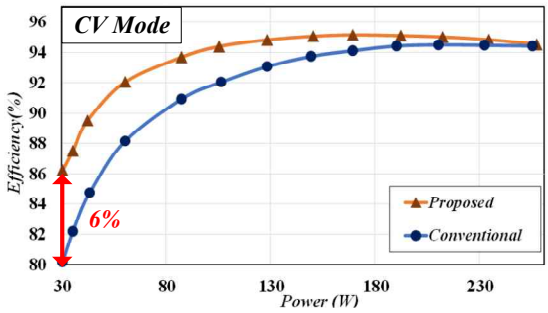

(b)

Fig. 13. Efficiency comparison result between the conventional LLC resonant converter and the proposed one: (a) CC mode and (b) CV mode

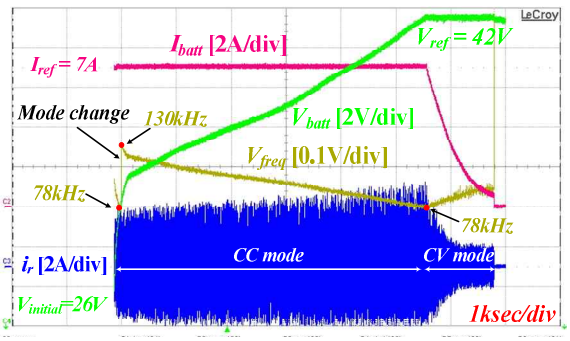

Fig. 14. Experiment waveforms during the CC-CV charging process

LLC resonant converter, the proposed one is superior to the conventional one over the entire operating range. The maximum efficiency of the CC charging process is 94.1%, which is 0.1% to 0.4% higher than that of the conventional one. The maximum efficiency of the CV charging process is 94.5%, which is 0.1% ~ 6% higher than the conventional one.

Fig. 14 displays the experimental waveform of CC-CV charging by applying the proposed converter. As can be seen from the figure, the CC-CV charging profile is appropriately implemented without any failures or unstable / unusable operation, despite the fact that a mode change occurred where the current reference of CCmode, I_{ref} is 7A, the voltage reference of the CV mode, V_{ref} is 42V, the

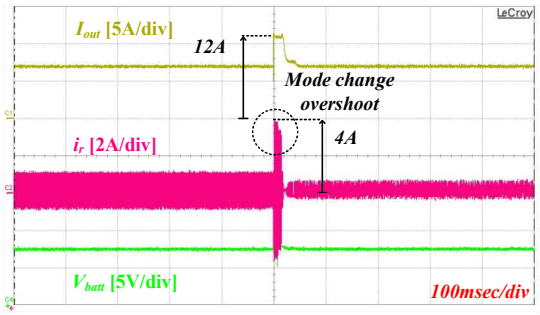

(a)

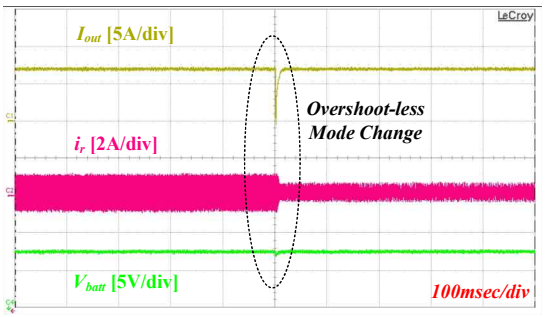

(b)

Fig. 15. Experiment waveforms under mode conversion: (a) without the overshoot-less algorithm and (b) with the overshoot-less algorithm

initial voltage of battery pack $V_{initial}$ is 26V, V_{freq} is a voltage value output by DAC converter to show the tendency of the switching frequency variation.

Fig. 15 displays waveforms related to when the overshoot elimination algorithm is and is not applied. As can be seen from the waveforms, when the overshoot elimination algorithm is not used, overshooting occurs in the resonance and output current. On the other hand, when the overshoot elimination algorithm is applied, mode conversion occurs without overshooting in either waveform. Therefore, it would be said that both the proposed converter with the adaptive turn ratio scheme operates well.

5. Conclusion

This paper proposes a high efficiency LLC resonant converter with a wide output voltage range using an adaptive turn ratio scheme for a 300W low power Li-ion battery charger. For a sequential description of the proposed method, this paper illustrates the operating principles and optimal design considerations of the proposed converter with topology analysis in detail. Finally, to verify the effectiveness of the proposed LLC resonant converter-based battery charger, experiments were conducted. Experimental results show that the proposed method operates reliably over a wide range of output voltages and achieves up to 6% more efficiently than conventional converter.

Acknowledgements

This work was supported by the Korea Institute of Energy Technology Evaluation and Planning (KETEP) and the Ministry of Trade, Industry & Energy (MOTIE) of the Republic of Korea (No. 20164010200860, No. 20168530050030).

References

[1] Yi-Hwa Liu, Jen-Hao Teng and Yu-Chung Lin, "Search for an optimal rapid charging pattern for lithium-ion batteries using ant colony system algorithm," *in Industrial Electronics, IEEE Transactions on*, vol. 52, no. 5, pp. 1328-1336, Oct. 2005

[2] A. A.-H. Hussein and I. Batarseh, "A review of charging algorithms for nickel and lithium battery chargers," *IEEE Trans. Veh. Technol.*, vol. 60, no. 3, pp. 830-838, Mar. 2011.

[3] Yang, B., Lee, F.C., Zhang, A.J. and Guisong Huang, "LLC resonant converter for front end DC/DC conversion," *in Proceedings of IEEE APEC*, pp. 1108-1112, Aug. 2002.

[4] B. Yang, "Topology investigation for front end DC/DC power conversion for distributed power system," *Virginia Polytechnic Inst. State Univ., Ph.D. dissertation*, 2003.

[5] H. Choi, "Analysis and Design of LLC Resonant Converter with Integrated Transformer," *in Proceedings of IEEE APEC*, pp.1630-1635, May 2007

[6] B. Lu, W. Liu, Y. Liang, F. C. Lee, and J. D. van Wyk, "Optimal design methodology for LLC resonant converter," *in Proceedings of IEEE APEC*, pp. 533-538., Mar. 2006

[7] R. Beiranvand, B. Rashidian, M. R. Zolghadri, and S. M. H. Alavi, "Optimizing the Normalized Dead-Time and Maximum Switching Frequency of a Wide-Adjustable-Range LLC Resonant Converter," *IEEE Trans. Power Electronics*, vol. 26, pp. 462-472, Aug. 2011.

[8] R. Beiranvand, B. Rashidian, M. R. Zolghadri, and S. M. H. Alavi, "A Design Procedure for Optimizing the LLC Resonant Converter as a Wide Output Range Voltage Source," *IEEE Trans. Power Electronics*, vol. 27, pp. 3749-3763, Feb. 2012.

[9] F. Musavi, M. Craciun, D. S. Gautam, W. Eberle, and W. G. Dunford, "An LLC Resonant DC/DC Converter for Wide Output Voltage Range Battery Charging Applications," *IEEE Trans. Power Electronics*, vol. 28, pp. 5437-5445, Mar. 2013.

[10] H. Wang, S. Dusmez, and A. Khaligh, "Design and Analysis of a Full-Bridge LLC-Based PEV Charger Optimized for Wide Battery Voltage Range," *IEEE Trans. Vehicular Technology*, vol. 63, pp. 1603-1613, Nov. 2014.

[11] Z. Fang, T. Cai, S. Duan, and C. Chen, "Optimal Design Methodology for LLC Resonant Converter in Battery Charging Applications Based on Time-Weighted Average Efficiency," *IEEE Trans. Power Electronics*, vol. 30, pp. 5469-5483, Dec. 2015.

[12] K. H. Park, Y. J. Choi, S. Y. Choi, and R. Y. Kim, "Design consideration of CC-CV controller of LLC resonant converter for Li-ion battery charger," *in Proceedings of IEEE IFEEC,* pp. 1-6, Nov. 2015.

[13] M. Y. Kim, B. C. Kim, K. B. Park and G. W. Moon, "LLC series resonant converter with auxiliary hold-up time compensation circuit," *in Proceedings of IEEE ECCE Asia (ICPE & ECCE),* pp. 628-633, Jul. 2011

[14] I. O. Lee, "Hybrid PWM-Resonant Converter for Electric Vehicle On-Board Battery Chargers," *IEEE Trans. Power Electronics*, vol. 31, pp. 3639-3649, Jul. 2016.

[15] J. S. Lai, H. Miwa, W. H. Lai, N. H. Tseng, C. S. Lee, C. H. Lin and Y. W. Shih, "A high-efficiency on-board charger utilizing a hybrid LLC and phase-shift DC-DC converter," *in Proceedings of IEEE IGBSG,* pp. 1-8, 2014.

[16] H. Choi, "Design consideration of half-bridge LLC resonant converter," *Journal of Power Electronics*, vol. 1, no. 1, pp. 13-20, Jun. 2007.

[17] Ya Liu, "High Efficiency Optimization of LLC Resonant Converter for Wide Load Range," *Virginia Polytechnic Inst. State* Univ., Master. dissertation, 2007.

Yeong-Jun Choi He received B.S degree in electrical and control engineering from Hanyang University, Seoul, Korea, in 2013, where he is currently working toward the direct Ph.D. degree. His current research interests include resonant converter, power factor correction converter and battery cell balancing circuit.

Hyeong-Gu Han He received B.S degree in Department of Control and Instrumentation Engineering from Korea National University of Transportation, in 2015 and the M.S. from electrical engineering from Hanyang University, Seoul, Korea, in 2017. Since 2017, He has been an engineer at LG electronics CTO division. His current research interests are resonant converter and battery charger.

See-Young Choi He received the B.S. and M.S. degrees in electrical engineering from Hanyang University, Seoul, Korea, in 1999 and 2001, respectively, where he is currently working toward the Ph.D. degree. From 2001 to 2006, he was a Senior Researcher at Hyosung Heavy Industry R&D Center, Seoul. From 2006 to 2014, he was a Senior Researcher at Samsung electronics. His current research interests are renewable energy, micro grid and resonant converter.

Sang-Il Kim He was born in Korea in 1975. He received the B.S., M.S. and the Ph.D degrees in electrical engineering from Hanyang University, Korea, in 1998, 2000 and 2017 respectively. From 2000 to 2005, he was a Researcher with POSCON Company, Korea. From 2005 to 2008, he was a member of the research staff at Samsung Advanced Institute of Technology, Yongin, Korea. Since 2008, he has been a Chief Research Engineer at Doosan Robotics Company, Seoul, Korea. His current research interests are power electronics control of electric machines, sensorless drives, electric/hybrid vehicle, and power conversion circuits.

Rae-Young Kim He received the B.S. and M.S. degrees from Hanyang University, Seoul, Korea, in 1997 and 1999, respectively, and the Ph.D. degree from Virginia Polytechnic Institute and State University, Blacksburg, VA, USA, in 2009, all in electrical engineering. From 1999 to 2004, he was a Senior Researcher at the Hyosung Heavy Industry R&D Center, Seoul, Korea. In 2009, he was a Postdoctoral Researcher at National Semiconductor Corporation, Santa Clara, CA, USA, involved in a smart home energy management system. In 2016, he was a Visiting Scholar with the Center for Power Electronics Systems (CPES), Virginia Polytechnic Institute and State University, Blacksburg. Since 2010, he has been with Hanyang University, where he is currently an Assistant Professor in the Department of Electrical and Biomedical Engineering. His research interests include modeling and control of distributed power converter systems, soft-switching techniques, energy management systems in microgrid applications, modular power converter for renewable energies and motor drive systems. Dr. Kim was a recipient of the 2007 First Prize Paper Award from the IEEE IAS.